Edible Structurally Colored Plastics

Xu Ma, Baohu Wu, Lei Hou,* and Peiyi Wu*

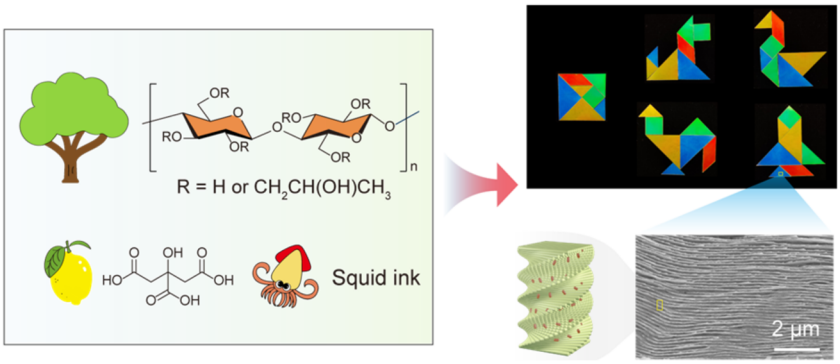

ABSTRACT: **Structurally colored plastics that no longer require dyes/pigments or additional dyeing processes are highly desirable for reducing environmental concerns. However, it remains challenging to fabricate such plastics with simultaneous brilliant structural colors, mechanical robustness, and convenient manufacturing, which are beneficial for their practical use. To address such an issue, we manipulate the cholesteric structures of a cellulose-derived liquid crystalline polymer, hydroxypropyl cellulose (HPC), thus realizing mechanically strong, room-temperature processable plastic substitutes with tunable structural color across the visible spectrum. By simply incorporating strong multiple hydrogen donors, such as citric acid, into the cholesteric pitch of the HPC mesophase, the reflected wavelength of the plastic can be linearly adjusted in the whole visible region. Meanwhile, the structurally colored plastics demonstrate excellent mechanical properties with tensile breaking strength of up to 72 MPa and Young's modulus of up to 1.6 GPa, comparable or superior to most commercial plastics. Moreover, the all-natural plastics can be facilely manufactured via three-dimensional (3D) printing, injection molding, origami, etc., and are readily recyclable and degradable. This work provides an effective path for the design of ecofriendly plastic substitutes from a whole-life perspective.**

KEYWORDS: *hydroxypropyl cellulose, structural color, cholesteric liquid crystal, hydrogen bond, mechanical robustness*

INTRODUCTION

Nowadays, the massive production of plastics all over the world is causing a heavy environmental burden,[1,2] thus making the development of sustainable plastics a critical issue.[3,4] Apart from the polymer matrix, a variety of additives in the plastic also contribute greatly to the environmental concerns,[5] from both carbon footprint and ecosystem health aspects. Among diverse additives, colorants, including dyes, pigments, as well as additives for internally colored plastics present one of the most frequently used additives in plastics.[6] Side effects of colorants in plastics on the environment lie in the following: (i) during manufacturing, current colorants are largely produced from fossil resources and coloring processes are energy-consuming, thus contributing to an increased share of global CO_2 emission; (ii) dyes and pigments are mostly toxic and would be released from the polymer matrix, thus bringing risks to organisms when plastics are left behind in lands or oceans; (iii) compositions and properties of colorants vary with each color, thus making the removal of colorants from plastics a difficult task during plastic recycling.[7] Under such circumstances, if the plastics themselves can display various vivid colors in the absence of colorants, doors will open for fully sustainable plastics.[8,9] Structural color, originated from the interaction of light with a periodic alternation of refractive indexes that results in Bragg's diffraction and reflection of a specific wavelength,[10,11] can be powerful in this context if properly used. In addition to avoiding the use of toxic dyes/pigments,

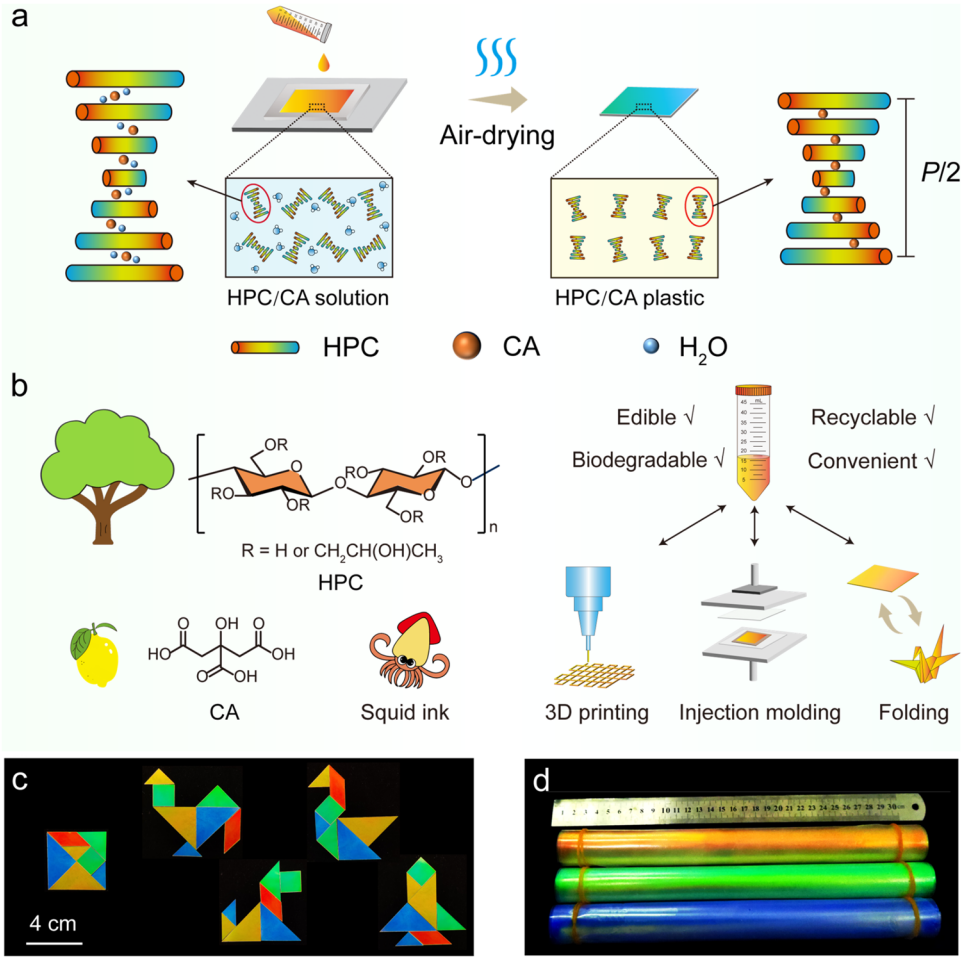

Figure 1. Fabrication of structurally colored HPC plastics: (a) schematic images of HPC/CA aqueous solution before and after air-drying; (b) raw materials and processing methods for structurally colored HPC/CA plastics; (c) processing HPC/CA plastics into tangram toys with diverse colors; (d) large-scale preparation of HPC/CA plastics.

structural color demonstrates convenient modulation as well as excellent long-term stability free from bleaching or fading benefited from that the reflected wavelength is dependent on dimensions of the periodic nanostructure,[12] rather than the specific absorption of dye or pigment molecules.[13] Meanwhile, ideal structurally colored plastic from a sustainable perspective needs to meet the following criteria: (i) structural color is derived from the inherent nature of the polymer matrix instead of relying on the incorporation of nanoparticles or complicated micro/nano-fabrication,[14,15] (ii) ease of processing and recycling; (iii) nontoxicity to both humans and the environment; (iv) crucially, retaining the essential properties of plastics, such as mechanical robustness. Hydroxypropyl cellulose (HPC), a cost-effective, edible, and highly biocompatible cellulose ether that has been widely used in food[16] and pharmaceutical industries,[17] can form a cholesteric liquid crystalline phase in a wide range of polar solvents,[18] including water, and display visible, iridescent structural colors,[19,20] presenting an excellent candidate for sustainable colored plastics.[21,22] However, structural colors of HPC are mostly observed in flowable solutions[23−25] or viscoelastic gels,[26−28] instead of glassy solid. This is because the reflected wavelength would blue-shift into ultraviolet region during solvent losing, finally leading to a completely transparent solid film.[29,30] Though attempts have been made to preserve the structural color of HPC in the solid state, such as kinetic trapping[31] and chemical cross-linking,[30,32−35] the mesophase of HPC in solutions is only kinetically arrested, thus making it difficult to fine-tune the structural colors. In addition, those methods always involve high-temperature processing of viscous HPC solutions, which unavoidably leads to the formation of many bubbles in the final films. Therefore, it is challenging to fabricate glassy HPC with bright structural colors for sustainable plastics. Here, we realize structurally colored HPC plastic using a molecular interaction-engineering strategy to manipulate the cholesteric structures of HPC in the solid state (Figure 1a). By simply introducing a biobased strong multiple hydrogen (H) donor, such as citric acid (CA), the HPC mesophase can be thermodynamically stabilized by strong H-bonds and will not collapse during the air-drying process, ultimately resulting in all-natural plastics with linearly tunable structural colors in the full spectrum of visible light. Particularly, the plastics are mechanically robust with breaking tensile strength of up to 72 MPa and Young's modulus of up to 1.6 GPa. Furthermore, we demonstrate that the plastics can be conveniently processed into diverse structures via three-dimensional (3D) printing, injection molding, origami, etc. (Figure 1b) and are readily recyclable with the assistance of water while maintaining structurally colored and robust. Moreover, the bioderived nature endows the plastic with excellent biodegradability. This work establishes a closed-loop system of edible structurally colored glassy HPC, providing a

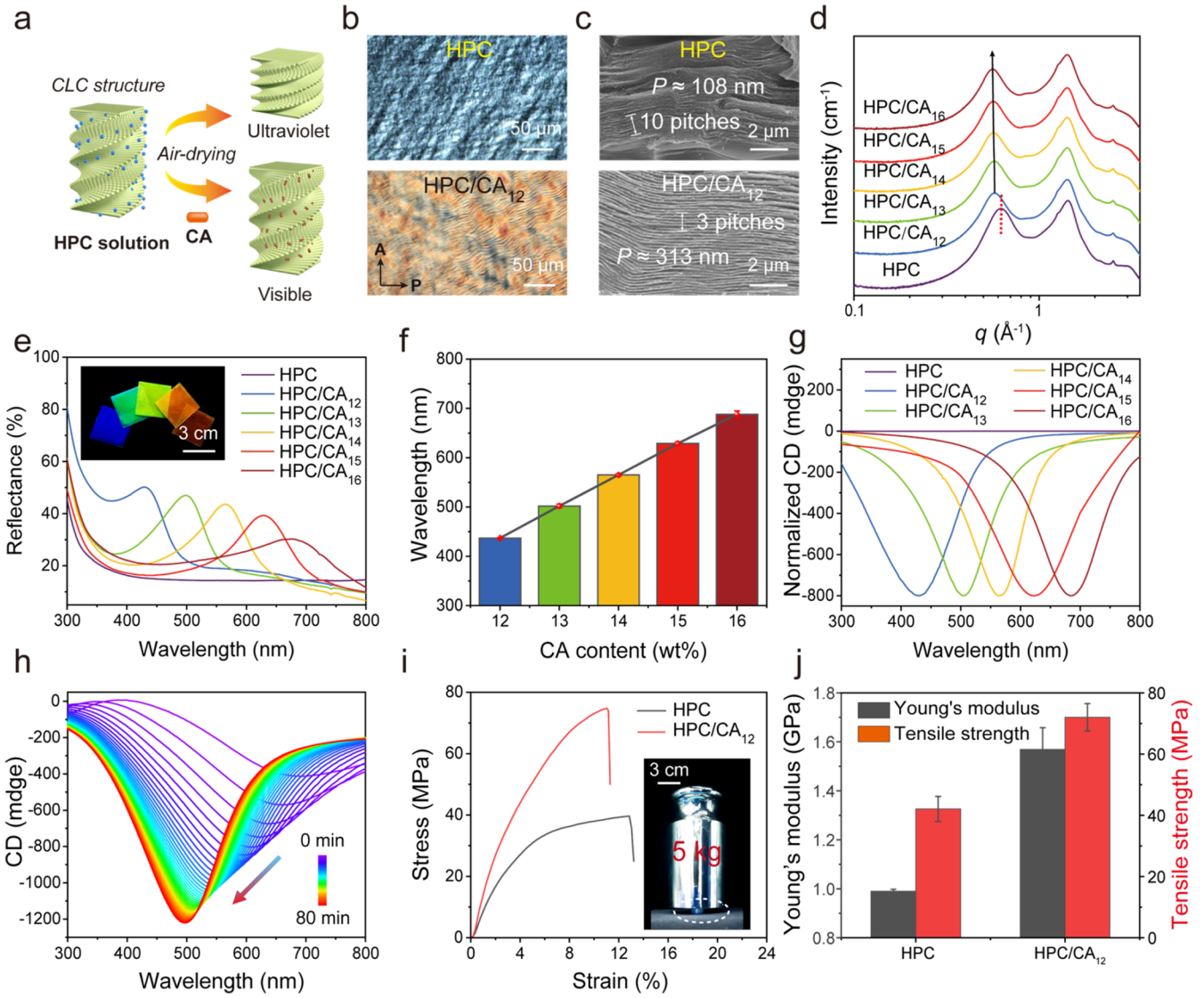

Figure 2. Evaluation of structure color and mechanical properties of HPC/CA plastics: (a) A schematic diagram of the helicoidal nanostructures before and after drying with or without CA; (b) POM images and (c) SEM images of HPC and HPC/CA_{12} plastics; (d) SAXS profiles of HPC and HPC/CA plastics; (e) the reflectance spectra of HPC/CA plastics and (f) the linear relationship between the reflected wavelength and CA content; (g) CD spectra of HPC and HPC/CA plastics; (h) time-dependent CD spectra of HPC/CA_{12} during water evaporation; (i) tensile stress−strain curves of HPC and HPC/CA_{12} (the inset shows the load-bearing capacity) as well as their calculated Young's modulus and tensile strength (j) equilibrated under 10% RH.

paradigm for the development of fully sustainable plastics toward a circular economy.

RESULTS AND DISCUSSION

Fabrication of Structurally Colored HPC Plastics. In concentrated aqueous solutions (e.g., 56−60 wt %), HPC can self-assemble into helicoidal nanostructures to form cholesteric mesophases, thus exhibiting structural colors from red to blue depending on the specific concentration, where higher concentrations lead to blue shift (Figure S1). Meanwhile, the HPC film is transparent after water evaporation due to the collapse of the cholesteric mesophase (Figure S2). Typically, the reflected wavelength of the cholesteric liquid crystal is determined by the nanostructure periodicity, material refractive index, and viewing angle, as defined by Bragg's reflection (eq 1) as followed[36]:[36]

$$\lambda = n\, p \cos\theta \tag{1}$$

where P is the helical pitch where the chiral vector rotates by 360 °, n is the average refractive index of the material, and θ is the angle between incident light and the cholesteric helix axis. To thermodynamically preserve the structural color in the visible light region, the key is to manipulate the cholesteric pitch of HPC in the glassy state. To do so, we introduced a third, physically interacting component into HPC aqueous solutions. There are several requirements when choosing such a third component: (i) showing suitable molecular size and holding strong interaction with HPC chains to insert into the cholesteric layers after drying; (ii) nonvolatile during water evaporation; (iii) not disrupting the assembling behavior of HPC in water. Considering that H-bonding interaction is essential during the solvent-induced cholesteric self-assembly of HPC,[18] we try to employ strong H-bonding agents as the physical stabilizer of HPC cholesteric layers during water removal. As shown in Figure S3, the ether and hydroxyl groups

in HPC structural units show a more negative electrostatic potential (ESP) and could serve as H-acceptors for H-bonding. Density functional theory (DFT) calculations indicate that, among various typical H-donors, including alcohols, amines, and carboxyl acids, carboxyl acids demonstrate the lowest binding energy with HPC, suggesting the strongest H-bonding tendency. Experimentally, we incorporated several typical H-donors (Figure S4) into concentrated HPC aqueous solutions to evaluate their capability to retain the structural color upon drying. As observed, only those dried HPC films integrated with carboxyl acid group-bearing molecules exhibit vivid structural colors (Figure S5), which parallels with the DFT results. Citric acid (CA), a tricarboxylic acid discovered from lemon,[37] is chosen as the representative for a detailed study to fabricate all-natural glassy HPC plastics with structural colors. Herein, the food-grade squid ink is added as a broadband absorber to enhance the saturation of the structural color while maintaining the edibility of HPC plastics. As shown in Figure S6, the incorporation of CA in the 60 wt % HPC aqueous solution results in a red shift of the structural color. Furthermore, reflection spectra of HPC aqueous solutions showed an increase in the maximum reflection wavelength with increasing CA content, indicating the expanding of helical pitch of the HPC cholesteric mesophase.[38,39] This behavior, to some extent, suggests that the CA molecule could be inserted into HPC cholesteric layers. In addition, the viscosity of the solution increases with the CA content, further implying the interaction between CA and HPC chains (Figure S7). The shear rate-dependent viscosity of all solutions displays the typical three characteristic regions of lyotropic liquid crystals,[40] where a distinct plateau region (Region II) separates two shear-thinning regions (Regions I and III) apart, revealing that CA does not hinder the development of cholesteric mesophase. Moreover, such a shear-thinning behavior of HPC/CA aqueous solutions will benefit additive manufacturing applications such as 3D printing. HPC-based plastics of diverse bright structural colors can be facilely obtained after air-drying HPC/CA aqueous solutions. As a proof of concept, the colored HPC/CA plastics can be used to produce tangram toys (Figure 1c), which demonstrate similar properties of commercial ones. Impotently, these toys are super safe for children due to the edible nature of HPC/CA plastics. Moreover, the method allows for large-scale production of defect-free structurally colored HPC/CA plastics, even under laboratory conditions (Figure 1d).

Evaluation of the Colors and Mechanical Properties of HPC/CA Plastics. The presence of CA in HPC aqueous solutions prevents the severe contraction of HPC cholesteric pitch that leads to a broad shift of the reflected wavelength into the ultraviolet region upon water evaporation. As shown in Figure 2b, the polarized optical microscope (POM) image of the air-dried HPC/CA plastic displays a typical fingerprint pattern associated with long-pitch cholesteric structure, whereas the pure HPC film demonstrates abruptly decreased fingerprint line spacings that are hardly resolvable in the optical microscope.[41] This can be further confirmed in scanning electron microscopy (SEM) images, where long-range continuous interlayers of the cholesteric materials can be directly observed (Figures 2c and S8). Compared with the pure HPC film, HPC/CA films exhibit obviously larger P values. Moreover, higher CA content in the plastic leads to larger P values, consequently causing a red shift of the plastics' structure color. The microstructure of HPC/CA plastics is investigated using small-angle X-ray scattering (SAXS). As shown in Figure 2d, all of the HPC/CA plastics exhibit similar scattering peaks with pure HPC film, suggesting that the liquid crystalline structure of HPC is preserved with the introduction of CA. Through more careful examination, we observed that the scattering peak around 0.62 $Å^{-1}$, which corresponds to the lateral spacing for interchain correlation between HPC molecules in the crystalline phase,[42−44] is apparently lower for HPC/CA plastics than that for pure HPC film. In addition, higher CA content leads to slightly lower q values. Under such a circumstance, it revealed that CA molecules could be inserted into the nematic layer stacking in the HPC mesophase. For the plastics containing 12−16 wt % CA, the structure color could cover the whole visible light from red to blue with reflected a wavelength between 691 and 434 nm (Figure 2e,f). On the equation mentioned above, the P values of HPC/CA plastics with varied CA content can be calculated. As displayed in Figure S9, increasing the CA content from 12 to 16 wt % leads to the P value changing from 290 to 460 nm, which parallels well with the SEM results. Herein, it is noted that a nearly linear increase in the reflected wavelength with CA contents can be observed, providing a convenient way to accurately tune the helical pitch of HPC-based plastic and achieve plastics with diverse structural colors. Circular dichroism (CD) spectroscopy is further utilized to examine the chiral assembly of HPC chains in the plastics. In Figure 2g, the chirality of cholesteric structure in HPC/CA plastics can be identified, suggesting that CA does not inhibit the assembling behavior of HPC chains. In addition, higher CA content leads to longer wavelengths of the CD signals, which is also consistent with results in reflection spectra. Observing that the pure HPC film exhibits a CD signal around 195 nm (Figure S10), it is confirmed that the presence of CA could prevent the helical pitch of the HPC cholesteric phase from drastic contraction after drying. Furthermore, we employ CD spectroscopy to in situ monitor the chiral assembly of HPC chains during air-drying. In Figure 2h, the CD peak of the HPC/CA_{12} aqueous solution exhibits a gradual blue shift during air-drying, suggesting that water loss leads to contraction of the cholesteric pitch of the mesophase. Through careful inspection, it is noticed that the CD peak progressively intensifies in the negative direction, accompanied by a narrowing of the peak shape. Such a behavior could be attributed to further assembly of the cholesteric mesophase phase during water evaporation that results in an increased number of cholesteric domains oriented perpendicular to the incident light.[16,18] Herein, the HPC/CA_{12} aqueous solution does not fully dry within the testing duration, thus leading to a relatively longer wavelength of the CD peak compared with that of the HPC/CA_{12} aqueous plastic. In addition, we monitored the color change of HPC/CA_{12} and HPC aqueous solutions during air-drying. As displayed in Figure S11, the color of the HPC/CA_{12} aqueous solution gradually shifts from red to blue, whereas that of the pure HPC aqueous solutions, regardless of their initial color, exhibits a rapid blue shift into the ultraviolet region after drying, further demonstrating the role of CA in preserving the structural color of the plastic. Furthermore, we investigated the effects of drying temperature on the structural color of HPC/CA plastics. As shown in Figure S12, higher drying temperatures lead to an increase in the cholesteric pitch and consequently red shifts of the structure color of the HPC/CA_{12} plastic. In addition to vibrant colors, mechanical robustness is critical for the practical use of plastics. We evaluate the mechanical performance of HPC and

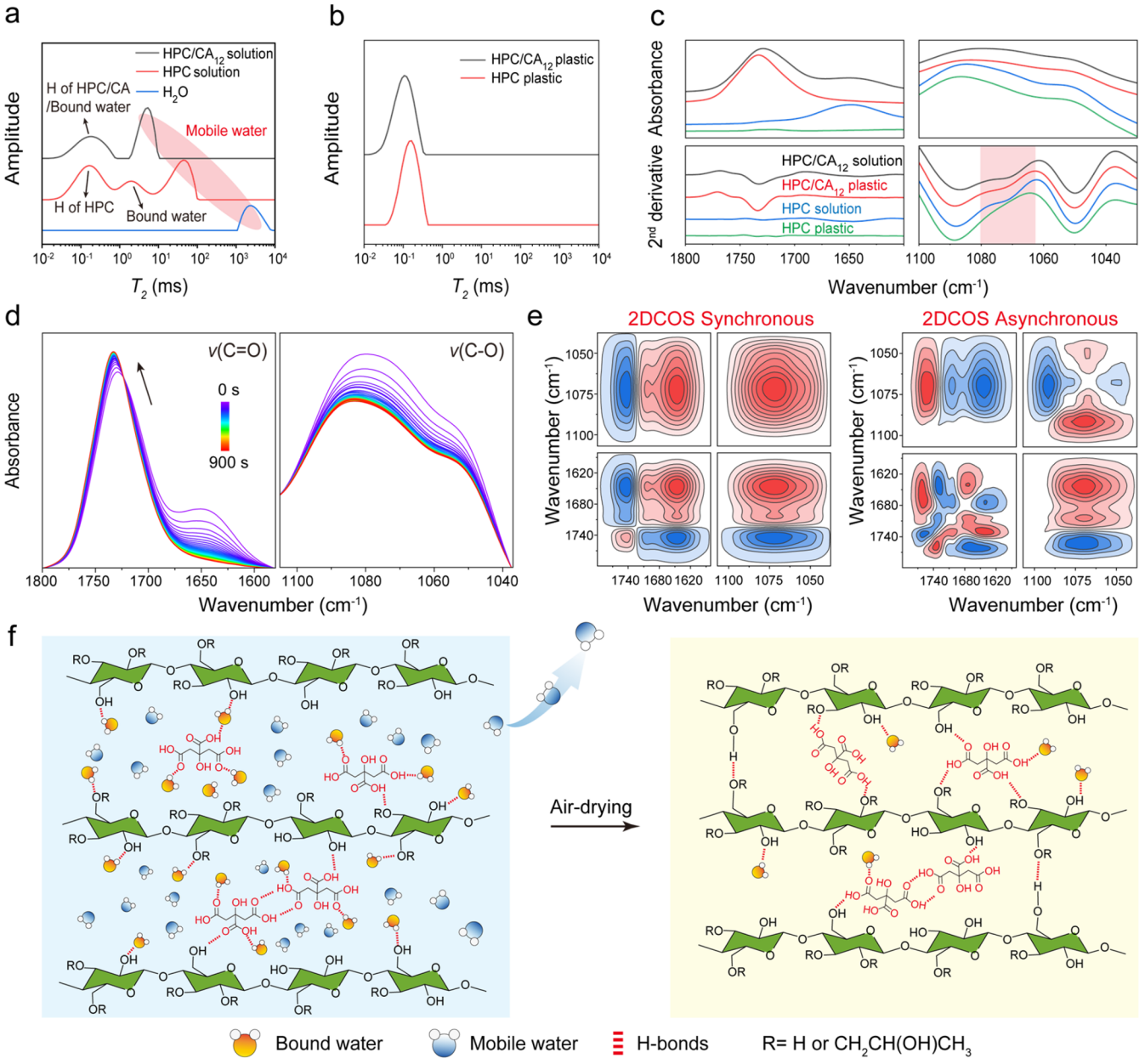

Figure 3. Molecular basis for structurally colored HPC/CA plastics: (a) LF ^{1}H NMR images of aqueous solutions of HPC/CA$_{12}$ and HPC as well as water; (b) LF ^{1}H NMR spectra of HPC/CA$_{12}$ plastic and pure HPC film; (c) contrast FTIR spectra of HPC/CA and HPC before and after air-drying as well as their corresponding second-derivative plots; (d) time-dependent FTIR spectra in the ν(C═O) and ν(C−O) regions during air-drying of an aqueous solution of HPC/CA$_{12}$; (e) 2Dcos synchronous and asynchronous spectra generated from (d). The warm colors (red) represent positive intensities, while cold colors (blue) represent negative ones; (f) a schematic diagram of the internal interactions of HPC/CA aqueous solution during air-drying.

HPC/CA plastics through uniaxial tensile tests. As shown in Figures 2i,j and S13a, the HPC/CA plastics exhibit significantly enhanced Young's modulus (E) and tensile breaking strength (σ_b) when compared with pure HPC film, which can be attributed to the physical cross-linking effect of CA. Meanwhile, a further increase in CA content leads to a slight decline in mechanical properties, which might be originated from the competition between plasticizing and cross-linking of CA to HPC chains.[45] It is noted that the HPC/CA plastics demonstrate E values of up to 1.6 GPa and σ_b values of up to 72 MPa, which are comparable or superior to most commercially available plastics (Figure S13b). The mechanical performance of the HPC/CA plastics is relatively sensitive to environmental humidity (Figure S14), where higher relative humidity (RH) leads to lower E due to water plasticizing. As shown in Figure S15a, the water content in the plastic increased from 0.9 to 17.5 wt % as RH changed from 10 to 90%. While the plastic is robust under ambient humidities. For instance, a 0.8 g HPC/CA$_{12}$ strip could bear a weight of 10 kg under 50% RH. Herein, the developed HPC/CA plastics not only feature tunable structural colors but also exhibit impressive mechanical properties, thus making them viable substitutes for traditional plastics. It is noted that the plastic exhibits a red shift in color with increasing RH (Figure S15b), which could originate from the expansion of HPC cholesteric pitch after moisture absorption.

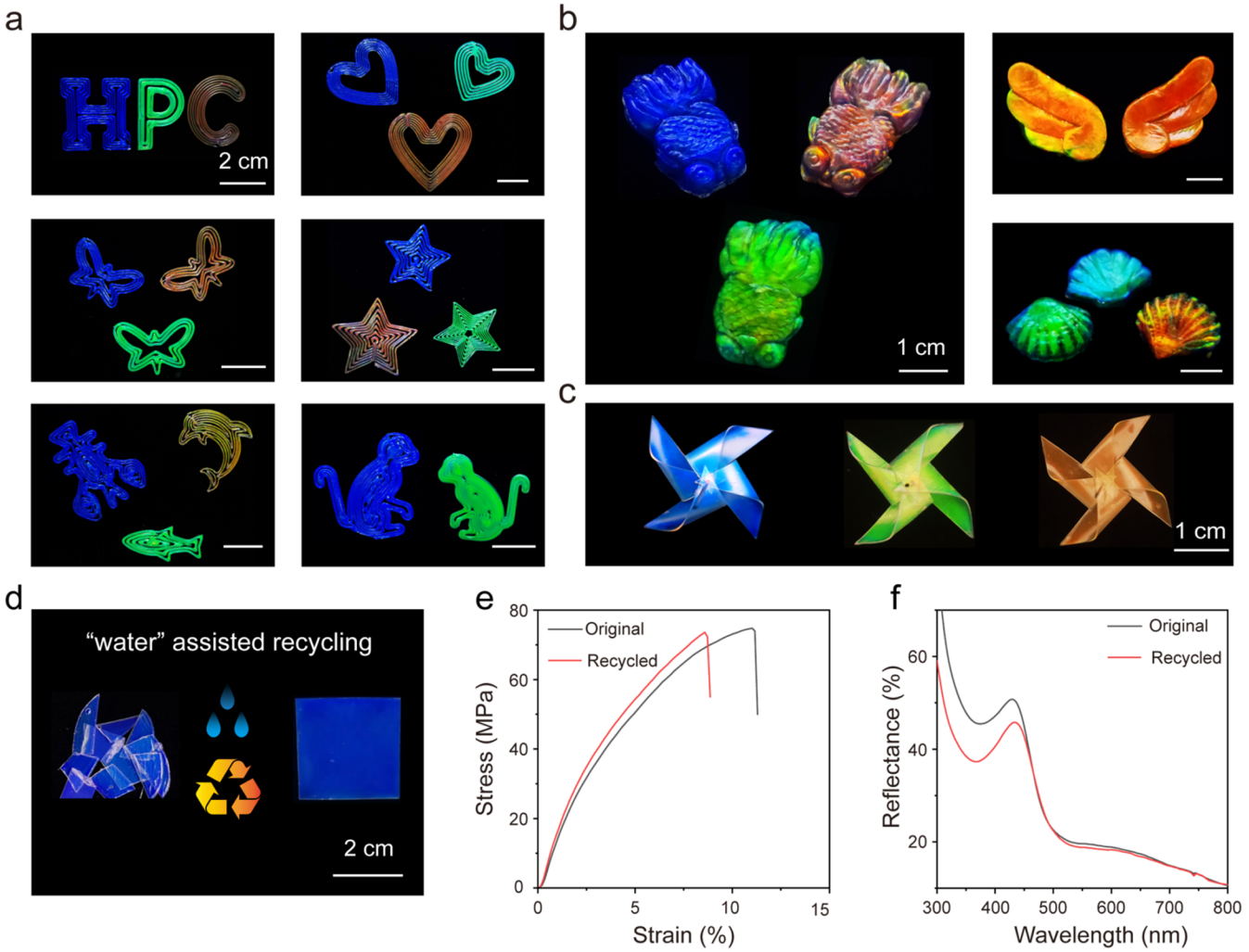

Figure 4. Processing and recycling of HPC/CA plastics. (a) Structurally colored patterns obtained by 3D printing and (b) three-dimensional structures obtained by injection molding technique; (c) origami was used to obtain the windmill structures; (d) water-assisted recycling of HPC/CA_{12} plastic; (e) tensile stress−strain curves and (f) reflection spectra of original and recycled HPC/CA_{12} plastic.

Molecular Basis for the Structurally Colored HPC/CA Plastics. We mainly employ low-field ^{1}H nuclear magnetic resonance (LF ^{1}H NMR) and infrared (IR) spectroscopy to elucidate the molecular mechanism governing the cholesteric structures of the HPC/CA plastics. As shown in Figure 3a, the spin−spin relaxation time (T_2) of protons in HPC and HPC/CA_{12} aqueous solutions has been measured by LF ^{1}H NMR. Generally, a higher T_2 value indicates a higher activity of the corresponding species.[46−48] For the HPC aqueous solution, the three T_2 peaks located at 43.3, 2.0, and 0.2 ms originate from mobile water, bound water, and HPC chains, respectively. After incorporating CA, the T_2 peak for mobile water shifts obviously toward a lower value. Meanwhile, the lower T_2 peak is relatively broad for HPC/CA aqueous solutions, which suggests that protons in bound water, CA, and HPC chains all exhibit similar activity. In addition, the two-dimensional (2D) LF ^{1}H NMR spectra, which provide a linear combination of longitudinal relaxation (T_1) and T_2 constants, are obtained to enhance the spectral resolution. Generally, lower T_1/T_2 ratios indicate high mobility and the diagonal line with T_1/T_2 = 1 represents a highly mobile liquid.[48,49] As shown in Figure S16, for the HPC aqueous solution, three peaks can be observed, which can be related to protons in mobile water, bound water, and HPC. Meanwhile, with CA content increasing, the signal of bound water gradually approaches and overlaps with the HPC/CA signal. Finally, only two peaks can be observed, where the more confined species with a higher T_1/T_2 ratio includes protons in HPC, CA, and bound water. Moreover, higher CA content leads to increased T_1/T_2 ratios of all of the protons in the solutions. Under such a circumstance, it is deduced that CA would interact with both HPC and water molecules and restrict their mobility. Furthermore, LF ^{1}H NMR is used to examine and compare the activity of protons in solid HPC and HPC/CA films. In Figure 3b, both systems exhibit only one T_2 value, hinting at the cooperative motions of all of the moieties in the solid state. Meanwhile, it is noted that the T_2 value in the solid HPC/CA is relatively lower than that in pure HPC, suggesting that protons are more confined in the HPC/CA system. Such behavior can also be confirmed from 2D LF ^{1}H NMR T_1-T_2 spectra of air-dried HPC and HPC/CA films (Figure S17). This observation, to some extent, might indicate that CA acts as a physical cross-linker for HPC chains, thus leading to decreased chain motions. Herein, interactions between CA and HPC not only contribute to the insertion of CA molecules in the cholesteric pitch to preserve structural color after drying but also benefit the enhanced mechanical

performance. It is noted that there is only a signal in both HPC and HPC/CA films during LF ^{1}H NMR measurements. To figure out whether CA entirely replaces the bound water, TGA analysis has been performed. As shown in Figure S18, both HPC and HPC/CA films show low water content after air-drying, with water content in HPC/CA being slightly higher than that in pure HPC. Such an observation can be attributed to the enhanced water retention with the presence of CA. Thus, it is inferred that the residing water is strongly bonded in the air-dried films and exhibits similar mobility with CA and HPC.

IR spectroscopy is additionally used to uncover the molecular interactions in the HPC/CA plastic. In this work, we mainly focus on two spectral regions, that is, C═O stretching (ν(C ═ O)) and O−H bending (δ(O−H)) regions (1780−1600 cm^{-1}) as well as C−O stretching (v(C−O)) region (1100−1030 cm^{-1}), to examine the specific interactions for all three components (CA, water, and HPC). First, IR spectra of aqueous HPC and HPC/CA solutions as well as air-dried HPC and HPC/CA plastics are compared in Figure 3c. Here, their second-derivative curves, where the sharpened minima are related to the maxima in the original absorption spectrum, are plotted to enhance the spectral resolution. For the v(C═O) band, a bule shift of the main peak at 1727 cm^{-1} has been observed after air-drying, demonstrating the dehydration of C═O groups. Meanwhile, two peaks located at 1703 and 1756 cm^{-1}, which can be related to dimeric hydrogen (H)-bonded and relatively free C═O groups, respectively, are less sensitive to air-drying, implying the existence of self-associated species of CA. In the v(C−O) region, the broad peak around 1090 cm^{-1} originates from the C−O−C stretching vibration in substituted hydroxypropyl groups along HPC chains. For the pure HPC system, a shoulder peak located at 1070 cm^{-1} is recognized for the aqueous HPC solution while disappearing after air-drying, suggesting that the shoulder peak can be assigned to C−O−C groups strongly H-bonded to water molecules. In stark contrast, the shoulder peak at around 1070 cm^{-1} exists in both aqueous HPC/CA solution and air-dried HPC/CA plastic. Such a behavior indicates that C−O−C groups are still in a strongly H-bonded state in the solid HPC/CA plastic. Considering that the COOH groups in CA are strong H-donors for H-bonding, we infer that the carboxyl acid-ether H-bond between CA and HPC plays the key role for the structural color and mechanical robustness of HPC/CA plastics. Time-dependent IR spectroscopy is utilized to monitor the chemical group changes during air-drying of aqueous HPC/CA solution. As displayed in Figure 3d, the intensity of δ(O−H) band at ∼1640 cm^{-1} decreases gradually to nearly 0 after air-drying, confirming the evaporation of water molecules. In the meantime, both v(C═O) and v(C−O−C) bands exhibit a slight blue shift during air-drying, suggesting the dehydration of C═O and C−O−C groups. Furthermore, 2D correlation spectroscopy (2Dcos), consisting of synchronous and asynchronous spectra (Figure 3e), is generated from time-dependent IR spectra to extract more subtle information about the interaction changes. Based on Noda's rule,[50] the sequential order of specific chemical groups during the air-drying process can be determined as follows: 1068 → 1090 → 1050 → 1732 → 1674 → 1637 → 1759 cm^{-1} ("→" means prior to or earlier than), i.e., v(C−O−C) (H-bonded to CA) → v(C−O−C) (relatively free) → v(C−OH) → v(C═O) (H-bonded to water) → δ(O−H) (mobile water) → δ(O−H) (bound water) → v(C═O) (relatively free). Altogether, the earlier response of v(C−O−C) (H-bonded to CA) highlights the predominant role of H-bonds between CA and HPC in plastic formation. As for water molecules, the mobile water evaporates prior to the bound ones, suggesting the gradual dehydration process. It is worth noting that a small amount of bound water still remains in the structurally colored plastics after air-drying. For clarity, a schematic illustration of H-bonding evolution during air-drying of an aqueous HPC/CA solution is displayed in Figure 3f.

Sustainable Processing and Recycling Properties of HPC/CA Plastics. HPC/CA plastics exhibit exceptional and convenient processability. Thanks to the shear-thinning rheological behavior of HPC/CA aqueous solutions, plastics with diverse patterns can be facilely fabricated through extrusion-based 3D printing. As shown in Figure 4a, various structural-color graphics can be printed, such as English letters, stars, and animals. Herein, the colors can be simply adjusted by CA content in the initial inks. Additionally, using a molding technique, air-drying of HPC/CA solutions in the molds with various shapes produces colorful three-dimensional structures, such as goldfish, shells, and wings (Figure 4b). Furthermore, the HPC/CA plastics can be softened and foldable under a humid environment, thus endowing the plastic with origami processing into complexed structures, such as a windmill and crane in Figures 4c and S19. Furthermore, owing to the supramolecular structure of the structurally colored plastics, which are dynamically cross-linked by hydrogen bonding, HPC/CA plastics can be facilely recycled with the assistance of water (Figure 4d). Specifically, at the end of their service life, adding a suitable amount of water followed by thorough mixing reforms the HPC/CA aqueous solution for reuse. Herein, the mechanical performance and structural color of the recycled HPC/CA plastics remain nearly unchanged (Figure 4e,f). Moreover, the use of all biobased feedstocks of the HPC/CA plastic endows them with excellent biodegradability (Figure S20), realizing a perfect closed-loop system that originates from and ultimately returns to nature.

CONCLUSIONS

In summary, we have developed a molecular interaction-engineering strategy for the design of robust structurally colored plastic that minimizes the environmental impact of using dyes and pigments. This strategy features the manipulation of cholesteric structures in solid HPC, an edible cellulose ether mostly forming a liquid crystalline mesophase in solutions. Through introducing a bioderived strong H-donor with a suitable molecular size, such as CA, the solid HPC mesophase can be thermodynamically stabilized in a proper cholesteric pitch with a reflected wavelength in the visible region. Particularly, a nearly linear relationship between CA content and reflected wavelength has been achieved, which provides a convenient way to accurately tune the structural colors of the sustainable plastic. Moreover, the HPC/CA plastics exhibit excellent mechanical performance with tensile breaking strength of up to 72 MPa and Young's modulus of up to 1.6 GPa, comparable or superior to most commercial plastics and beneficial for their practical use. In addition, the HPC/CA plastic can be facilely processed into diverse structures via 3D printing, injection molding, origami, etc. and is readily recyclable and degradable. This work provides an efficient strategy for the development of colorant-free plastics with bright colors, contributing to a sustainable future.

EXPERIMENTAL SECTION

Materials. Hydroxypropyl cellulose (HPC, 3−6 mPa·s in 2% aqueous solution at 20 °C; M_w = 92,000 g·mol^{-1} and PDI = 2.2, determined with GPC; molar substitution (MS) of 3.9, determined by ^{1}H NMR) was purchased from Tokyo Chemical Industry (Japan). Citric acid (CA) was purchased from Sigma-Aldrich. Squid powder, consisting of squid ink sacs, gum arabic, and maltodextrin, was purchased at local markets. All chemicals were used as received without any further purification or modification.

Preparation and Processing of HPC/CA Plastics. HPC/CA plastics were achieved by air-drying HPC/CA solutions with varied CA and water contents, where the mass ratio of HPC was fixed at 60 wt %. Typically, for HPC/CA_{12} plastic, 6.0 g of HPC, 2.8 g of water (containing 0.1 wt % squid powder), and 1.2 g of CA were physically mixed in the Thinky ARE-310 planetary centrifugal mixer. Then, the mixed viscous solution was centrifuged for 30 min at 10,000 rmp/min to remove bubbles and further transferred into a poly(tetrafluoroethylene) (PTFE) mold for air-drying (∼30% RH and 25 °C). For 3D printing, the HPC/CA solutions were centrifuged in 10 mL syringes before printing. 3D printing of the plastic was conducted on Regenovo 3D Bio-Architect SR. For injection molding, the viscose HPC/CA solutions were placed in a special mold, and the plastics were released from the mold after air-drying. For origami, HPC/CA films are processed into various structures under a humid environment (provided by a humidifier) and subsequently transferred to ambient humidity to fix the shape. For plastic recycling, by dissolving plastic pieces of HPC/CA into aqueous solutions with an HPC content of 60 wt %, the plastic can be reobtained after air-drying. Taking the recycling process of HPC/CA_{12} plastic as an example, ∼0.88 g of water is added to the plastic pieces weighing ∼2.36 g. Then, the aqueous solution can be reformed after thorough mixing. Finally, the blue HPC/CA_{12} plastic is obtained after air-drying.

Materials Characterizations. POM images of HPC and HPC/CA plastics were observed under crossed polarizers with a λ plate on a polarization optical microscope (DM2500P, Leica). The cross-sectional images were obtained by SEM (Hitachi, Japan SU8230). Samples were sputter-coated with gold before imaging (60 mA for 120 s). The small-angle X-ray scattering (SAXS) experiments were conducted at the JCNS MLZ using a laboratory-based SAXS beamline, KWS-X (XENOCS XUESS 3.0 XL). A MetalJet X-ray source (Excillum D2+) with a liquid metal anode operated at 70 kV and 3.57 mA, emitting Ga Kα radiation with a wavelength (λ) of 1.314 Å. The reflection and circular dichroism spectra were collected on circular dichroism spectrometers (A66, Applied Photophysic, Inc.). Tensile tests were carried out on a universal testing machine (Instron 5966 two-column bench test system) at a strain rate of 0.1 s^{-1}. Relative humidity was controlled by a constant temperature and humidity chamber (KMF 115, German binder). When testing mechanical properties at different humidity, the samples were balanced at a fixed humidity for 6 h. LF ^{1}H NMR spectra were obtained by the NMR analyzer (VTMR20−010 V−I, Suzhou Niumag Analytical Instrument Corporation, China), where samples were sealed in the glass vial to avoid water evaporation during testing. Fourier transform infrared (FTIR) spectra were obtained in the transmission model on a Nicolet iS50 (Thermo Fisher Scientific) spectrometer. All of the time-variable FTIR spectra of the HPC/CA_{12} solution were used for performing 2D correlation analysis. 2D correlation analysis was carried out using the software 2D Shige, ver. 1.3 (©Shigeaki Morita, Kwansei Gakuin University, Japan, 2004−2005) and further plotted into contour maps by the OriginPro 2024 program. In the contour maps, red colors are defined as positive intensities, while blue colors as negative ones.

AUTHOR INFORMATION

Corresponding Authors

Lei Hou − *State Key Laboratory of Advanced Fiber Materials (Donghua University), College of Chemistry and Chemical Engineering, Center for Advanced Low-Dimension Materials, Donghua University, Shanghai 201620, China*; Email: houlei@dhu.edu.cn

Peiyi Wu − *State Key Laboratory of Advanced Fiber Materials (Donghua University), College of Chemistry and Chemical Engineering, Center for Advanced Low-Dimension Materials, Donghua University, Shanghai 201620, China*; orcid.org/0000-0001-7235-210X; Email: wupeiyi@dhu.edu.cn

Authors

Xu Ma − *State Key Laboratory of Advanced Fiber Materials (Donghua University), College of Chemistry and Chemical Engineering, Center for Advanced Low-Dimension Materials, Donghua University, Shanghai 201620, China*

Baohu Wu − *Jülich Centre for Neutron Science (JCNS) at Heinz Maier-Leibnitz Zentrum (MLZ) Forschungszentrum Jülich, 85748 Garching, Germany*; orcid.org/0000-0002-1291-8965

Author Contributions

L.H. and P.W. conceived the project. X.M. carried out all of the experiments. B.W. made the SAXS data analyses. All authors provided critical reviews and helped shape the research and analysis.

Notes

The authors declare no competing financial interest.

ACKNOWLEDGMENTS

This work was supported by the Fundamental Research Funds for the Central Universities (No. 2232025A-04), the National Natural Science Foundation of China (NSFC) (No.

52433003) and the Research Foundation of the National Innovation Center of Advanced Dyeing & Finishing Technology (No. 2022GCJJ07).

REFERENCES

(1) Pinheiro, H. T.; MacDonald, C.; Santos, R. G.; Ali, R.; Bobat, A.; Cresswell, B. J.; Francini-Filho, R.; Freitas, R.; Galbraith, G. F.; Musembi, P.; Phelps, T. A.; Quimbayo, J. P.; Quiros, T. E. A. L.; Shepherd, B.; Stefanoudis, P. V.; Talma, S.; Teixeira, J. B.; Woodall, L. C.; Rocha, L. A. Plastic Pollution on the World's Coral Reefs. *Nature* **2023**, *619*, No. 311316.

(2) On the Plastics Crisis (Editorial) *Nat. Sustain.* 2023; Vol. *6*, p 1137.

(3) Xia, Q.; Chen, C.; Yao, Y.; Li, J.; He, S.; Zhou, Y.; Li, T.; Pan, X.; Yao, Y.; Hu, L. A Strong, Biodegradable and Recyclable Lignocellulosic Bioplastic. *Nat. Sustain.* **2021**, *4*, 627−635.

(4) Li, X.-J.; Zhao, Y.; Tan, Q.; Han, Z.; Tang, B.; Wang, Y.; Song, F. Corn Straw Cellulose Nanocrystals: Preparation, Structural Coloration, and High-Level Anti-Counterfeiting. *Ind. Crops Prod.* **2025**, *224*, No. 120393.

(5) Zhang, L.; He, Y.; Jiang, L.; Shi, Y.; Hao, L.; Huang, L.; Lyu, M.; Wang, S. Plastic Additives As a New Threat to the Global Environment: Research Status, Remediation Strategies and Perspectives. *Environ. Res.* **2024**, *263*, No. 120007.

(6) Parker, R. M.; Zhao, T. H.; Frka-Petesic, B.; Vignolini, S. Cellulose Photonic Pigments. *Nat. Commun.* **2022**, *13*, No. 3378.

(7) Sánchez-Rivera, K. L.; Munguía-López, A. d. C.; Zhou, P.; Cecon, V. S.; Yu, J.; Nelson, K.; Miller, D.; Grey, S.; Xu, Z.; Bar-Ziv, E.; Vorst, K. L.; Curtzwiler, G. W.; Van Lehn, R. C.; Zavala, V. M.; Huber, G. W. Recycling of a Post-Industrial Printed Multilayer Plastic Film Containing Polyurethane Inks by Solvent-Targeted Recovery and Precipitation. *Resour., Conserv. Recycl.* **2023**, *197*, No. 107086.

(8) Droguet, B. E.; Liang, H.-L.; Frka-Petesic, B.; Parker, R. M.; De Volder, M. F. L.; Baumberg, J. J.; Vignolini, S. Large-Scale Fabrication of Structurally Coloured Cellulose Nanocrystal Films and Effect Pigments. *Nat. Mater.* **2022**, *21*, 352−358.

(9) Guidetti, G.; Atifi, S.; Vignolini, S.; Hamad, W. Y. Flexible Photonic Cellulose Nanocrystal Films. *Adv. Mater.* **2016**, *28*, 10042−10047.

(10) Wang, H.; Liu, Y.; Chen, Z.; Sun, L.; Zhao, Y. Anisotropic Structural Color Particles from Colloidal Phase Separation. *Sci. Adv.* **2020**, *6*, No. eaay1438.

(11) Zhang, Z.; Chen, Z.; Sun, L.; Zhang, X.; Zhao, Y. Bio-Inspired Angle-Independent Structural Color Films With Anisotropic Colloidal Crystal Array Domains. *Nano Res.* **2019**, *12*, 1579−1584.

(12) Esmaeili, M.; Norouzi, S.; George, K.; Rezvan, G.; Taheri-Qazvini, N.; Sadati, M. 3D Printing-Assisted Self-Assembly to Bio-Inspired Bouligand Nanostructures. *Small* **2023**, *19*, No. 2206847.

(13) Sealy, C. Structural Color Promises Energy-Saving Paint. *Nano Today* **2023**, *50*, No. 101866.

(14) Hong, W.; Yuan, Z.; Chen, X. Structural Color Materials for Optical Anticounterfeiting. *Small* **2020**, *16*, No. 1907626.

(15) Peng, L.; Hou, L.; Wu, P. Synergetic Lithium and Hydrogen Bonds Endow Liquid-Free Photonic Ionic Elastomer with Mechanical Robustness and Electrical/Optical Dual-Output. *Adv. Mater.* **2023**, *35*, No. 2211342.

(16) Parker, R. M.; Parton, T. G.; Chan, C. L. C.; Bay, M. M.; Frka-Petesic, B.; Vignolini, S. Bioinspired Photonic Materials from Cellulose: Fabrication, Optical Analysis, and Applications. *Acc. Mater. Res.* **2023**, *4*, 522−535.

(17) Jones, D. S.; Rafferty, G. P.; Andrews, G. P. Drug Release from Hydroxypropylcellulose Gels Cannot Be Statistically Predicted from Their Viscometric and Initial Viscoelastic Properties. *Carbohydr. Polym.* **2021**, *256*, No. 117512.

(18) Fine, S. G.; Chazot, C. A. C. Unraveling the Governing Mechanisms Behind the Chiral Nematic Self-Assembly of Cellulose-Based Polymers. *Chem. Mater.* **2023**, *35*, 8774−8787.

(19) Werbowyj, R. S.; Gray, D. G. Liquid Crystalline Structure in Aqueous Hydroxypropyl Cellulose Solutions. *Mol. Cryst. Liq. Cryst.* **1976**, *34*, 97−103.

(20) Gray, D. G. Chiral Nematic Ordering of Polysaccharides. *Carbohydr. Polym.* **1994**, *25*, 277−284.

(21) Frka-Petesic, B.; Vignolini, S. So Much More than Paper. *Nat. Photonics* **2019**, *13*, 365−367.

(22) Espinha, A.; Dore, C.; Matricardi, C.; Alonso, M. I.; Goñi, A. R.; Mihi, A. Hydroxypropyl Cellulose Photonic Architectures by Soft Nanoimprinting Lithography. *Nat. Photonics* **2018**, *12*, 343−348.

(23) Kamita, G.; Vignolini, S.; Dumanli, A. G. Edible Cellulose-Based Colorimetric Timer. *Nanoscale Horiz.* **2023**, *8*, 887−891.

(24) Yi, H.; Lee, S. H.; Ko, H.; Lee, D.; Bae, W. G.; Kim, Ti.; Hwang, D. S.; Jeong, H. E. Ultra-Adaptable and Wearable Photonic Skin Based on a Shape-Memory, Responsive Cellulose Derivative. *Adv. Funct. Mater.* **2019**, *29*, No. 1902720.

(25) Li, D.; Jiang, R.-R.; Chen, S.-K.; Wu, J.-M.; Dong, X.; Wang, X.-L.; Wang, Y.-Z.; Song, F. Rapid, Linear, and Highly Reliable Structural-Color Switching Enabled by Thermal Regulation of Chiral Nematic Mesophases. *Chem. Eng. J.* **2023**, *453*, No. 139835.

(26) Barty-King, C. H.; Chan, C. L. C.; Parker, R. M.; Bay, M. M.; Vadrucci, R.; De Volder, M.; Vignolini, S. Mechanochromic, Structurally Colored, and Edible Hydrogels Prepared from Hydroxypropyl Cellulose and Gelatin. *Adv. Mater.* **2021**, *33*, No. 2102112.

(27) Huang, L. Y.; Zhang, X. Z.; Deng, L.; Wang, Y.; Liu, Y. M.; Zhu, H. L. Sustainable Cellulose-Derived Organic Photonic Gels with Tunable and Dynamic Structural Color. *ACS Nano* **2024**, *18*, 3627−3635.

(28) Zhang, Z.; Chen, Z.; Wang, Y.; Zhao, Y. Bioinspired Conductive Cellulose Liquid-Crystal Hydrogels As Multifunctional Electrical Skins. *Proc. Natl. Acad. Sci. U.S.A.* **2020**, *117*, 18310−18316.

(29) Huang, Y.; Qian, Y.; Chang, Y.; Yu, J.; Li, Q.; Tang, M.; Yang, X.; Liu, Z.; Li, H.; Zhu, Z.; Li, W.; Zhang, F.; Qing, G. Intense Left-handed Circularly Polarized Luminescence in Chiral Nematic Hydroxypropyl Cellulose Composite Films. *Adv. Mater.* **2024**, *36*, No. 2308742.

(30) Chan, C. L. C.; Bay, M. M.; Jacucci, G.; Vadrucci, R.; Williams, C. A.; van de Kerkhof, G. T.; Parker, R. M.; Vynck, K.; Frka-Petesic, B.; Vignolini, S. Visual Appearance of Chiral Nematic Cellulose-Based Photonic Films: Angular and Polarization Independent Color Response with a Twist. *Adv. Mater.* **2019**, *31*, No. 1905151.

(31) George, K.; Esmaeili, M.; Wang, J.; Taheri-Qazvini, N.; Abbaspourrad, A.; Sadati, M. 3D Printing of Responsive Chiral Photonic Nanostructures. *Proc. Natl. Acad. Sci. U.S.A.* **2023**, *120*, No. e2220032120.

(32) Chan, C. L. C.; Lei, I. M.; van de Kerkhof, G. T.; Parker, R. M.; Richards, K. D.; Evans, R. C.; Huang, Y. Y. S.; Vignolini, S. 3D Printing of Liquid Crystalline Hydroxypropyl Cellulose—toward Tunable and Sustainable Volumetric Photonic Structures. *Adv. Funct. Mater.* **2022**, *32*, No. 2108566.

(33) Balcerowski, T.; Ozbek, B.; Akbulut, O.; Dumanli, A. G. Hierarchical Organization of Structurally Colored Cholesteric Phases of Cellulose via 3D Printing. *Small* **2023**, *19*, No. 2205506.

(34) Zhang, Z. H.; Wang, C.; Wang, Q.; Zhao, Y. J.; Shang, L. R. Cholesteric Cellulose Liquid Crystal Ink for Three-Dimensional Structural Coloration. *Proc. Natl. Acad. Sci. U.S.A.* **2022**, *119*, No. e2204113119.

(35) Zhang, Z.; Chen, Z.; Wang, Y.; Zhao, Y.; Shang, L. Cholesteric Cellulose Liquid Crystals with Multifunctional Structural Colors. *Adv. Funct. Mater.* **2021**, *32*, No. 2107242.

(36) Parton, T. G.; Parker, R. M.; Osbild, S.; Vignolini, S.; Frka-Petesic, B. Angle-Resolved Optical Spectroscopy of Photonic Cellulose Nanocrystal Films Reveals the Influence of Additives on the Mechanism of Kinetic Arrest. *Soft Matter* **2024**, *20*, 3695−3707.

(37) Zhang, W.; Roy, S.; Assadpour, E.; Cong, X.; Jafari, S. M. Cross-Linked Biopolymeric Films by Citric Acid for Food Packaging and Preservation. *Adv. Colloid Interface Sci.* **2023**, *314*, No. 102886.

(38) Li, D.; Wu, J.-M.; Liang, Z.-H.; Li, L.-Y.; Dong, X.; Chen, S.-K.; Fu, T.; Wang, X.-L.; Wang, Y.-Z.; Song, F. Sophisticated yet

Convenient Information Encryption/Decryption Based on Synergistically Time-/Temperature-Resolved Photonic Inks. *Adv. Sci.* **2023**, *10*, No. 2206290.
(39) Tan, Q.-W.; Li, D.; Li, L.-Y.; Wang, Z.-L.; Wang, X.-L.; Wang, Y.-Z.; Song, F. A Rule for Response Sensitivity of Structural-Color Photonic Colloids. *Nano Lett.* **2023**, *23*, 9841−9850.
(40) Esmaeili, M.; George, K.; Rezvan, G.; Taheri-Qazvini, N.; Zhang, R.; Sadati, M. Capillary Flow Characterizations of Chiral Nematic Cellulose Nanocrystal Suspensions. *Langmuir* **2022**, *38*, 2192−2204.
(41) Mitov, M. Cholesteric liquid crystals in living matter. *Soft Matter* **2017**, *13*, 4176−4209.
(42) Ma, L.; Wang, L.; Wu, L.; Zhuo, D.; Weng, Z.; Ren, R. Cellulosic Nanocomposite Membranes from Hydroxypropyl Cellulose Reinforced by Cellulose Nanocrystals. *Cellulose* **2014**, *21*, 4443−4454.
(43) Kuse, Y.; Asahina, D.; Nishio, Y. Molecular Structure and Liquid-Crystalline Characteristics of Chitosan Phenylcarbamate. *Biomacromolecules* **2009**, *10*, 166−173.
(44) Shi, H.; Yang, Y.; Huang, Y.; Li, X.; Shi, Y. Anisotropic Single-Domain Hydrogel with Stimulus Response to Temperature and Ionic Strength. *Macromolecules* **2023**, *56*, 528−534.
(45) Duarte, G. A.; Bezerra, M. C.; Bettini, S. H. P.; Lucas, A. A. Real-Time Monitoring of the Starch Cross-Linking with Citric Acid by Chemorheological Analysis. *Carbohydr. Polym.* **2023**, *311*, No. 120733.
(46) Gong, K.; Hou, L.; Wu, P. Hydrogen-Bonding Affords Sustainable Plastics with Ultrahigh Robustness and Water-Assisted Arbitrarily Shape Engineering. *Adv. Mater.* **2022**, *34*, No. 2201065.
(47) Xu, G. G.; Hou, L.; Wu, P. Y. Sustainable Plastics with High Performance and Convenient Processibility. *Adv. Sci.* **2024**, *11*, No. 2405301.
(48) Liu, Y.; Song, Y.; Wu, P. Self-Evolving Hierarchical Hydrogel Fibers with Circadian Rhythms and Memory Functions. *Adv. Mater.* **2024**, *36*, No. 2404506.
(49) Liu, Y.; Zhang, J.; Wu, P. Near-Frictionless Long-Distance Water Transport in Trees Enabled by Hierarchically Helical Molecular Pumps. *CCS Chem.* **2025**, *7*, 484−492.
(50) Noda, I. Generalized Two-Dimensional Correlation Method Applicable to Infrared, Raman, and other Types of Spectroscopy. *Appl. Spectrosc.* **1993**, *47*, 1329−1336.